Journal of
Materials Chemistry C

Materials for optical, magnetic and electronic devices

## Accepted Manuscript

This article can be cited before page numbers have been issued, to do this please use: N. Hizukuri, H. Imai and Y. Oaki, *J. Mater. Chem. C*, 2026, DOI: 10.1039/D6TC01280A.

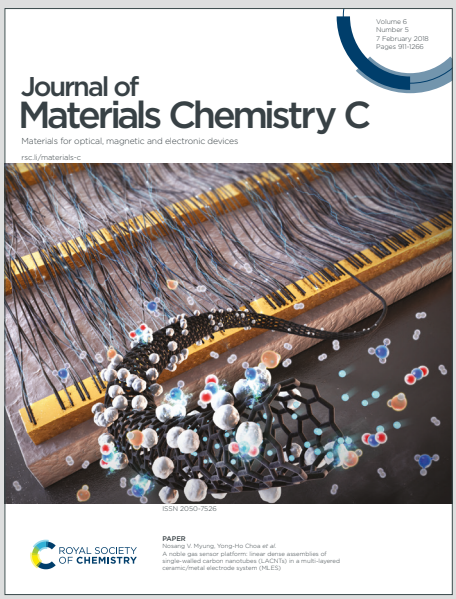




ROYAL SOCIETY OF CHEMISTRY

rsc.li/materials-c

Journal of Materials Chemistry C

View Article Online
DOI: 10.1039/D6TC01280A

PAPER

# Brilliant colors originating from weak reflections of an ill-defined inverse opal structure and its application as a humidity sensor

Naoki Hizukuri,[a] Yuya Oaki,[a] Hiroaki Imai*[a]

Received 00th January 20xx,
Accepted 00th January 20xx

DOI: 10.1039/x0xx00000x

www.rsc.org/

Ethiopian opal exhibits higher transparency and more vivid structural colors as compared to other opal varieties; however, the underlying mechanisms of these unique optical properties remain largely unexplained. This study analyzed the microstructure of Ethiopian opal, revealing that its vivid coloration results from the superposition of extremely weak reflections originating from a subtly defined inverse opal structure with submicron-scale periodicity. Regions of relatively high refractive indices exist in the cement parts between the gaps of arrayed submicron colloidal particles, creating highly transmissive and weakly reflective interfaces unique to this opal architecture. Interference across thousands of these weakly reflecting layers produces a sharp reflection spectrum with a narrow half-width. The colloidal particles were found to be comprised of silica nanograins approximately 20 nm in size and contain pores of about 6 nm as gaps among the nanograins. Because the refractive index of these particles shifts upon the condensation of water in the nanopores, the structural color exhibits a sensitive response to variations in humidity, demonstrating the potential of the Ethiopian opal architecture as a humidity sensor.

## Introduction

Structural colors observed in nature, such as those of morpho butterflies and jewel beetles, are derived from the diffraction, interference, and scattering of visible light by microstructures.[1–3] In particular, natural opal—formed by the self-assembly of monodisperse submicron colloidal silica particles into a face-centered cubic or hexagonal close-packed structure—is a classic example of a photonic crystal.[4–10] Due to their potential for cost-effective and simple solution-based fabrication, along with the relative ease of large-scale production, opals have attracted significant attention and have been extensively developed for use as light-control materials.[6,9–12] Consequently, elucidating the microstructure of natural opal is vital for establishing guidelines to control nanostructures through self-assembly.

Natural opals are typically classified as either sedimentary[13] or volcanic.[14] The former develops in sedimentary rocks over millions of years (e.g., Australian black opals), while the latter forms within voids in volcanic rocks like rhyolite (e.g., Mexican and Ethiopian opals). Although both processes involve the deposition and ordering of colloidal silica particles,[6, 15] their differing formation temperatures lead to amorphous Opal-A in sedimentary settings and partially crystalline Opal-C (cristobalite) / CT (cristobalite and tridymite) in volcanic environments.[16] In most opals, the substantial refractive index contrast between silica and the interstitial air causes strong reflection within the first few dozen layers, which inherently limits the transparency of the material.[17] In contrast, Ethiopian opal—a volcanic variety—is characterized by its vivid structural coloration paired with exceptional transparency.[14, 18] Despite these remarkable properties, the structural origin of its transparency remains largely unexplored.

Similar optical phenomena can be observed in biological systems. For instance, nacre exhibits a characteristic pearlescent luster due to multilayer interference.[19–21] Our recent study on certain fossil pearls has revealed that a unique "nanogap" structure facilitates vivid structural coloration by balancing high transmittance with low, yet precise, reflectance.[22] Given that Ethiopian opal shares this high transparency, it likely possesses a similar architecture that enables a narrow reflectance spectral width despite low individual interface reflectivity. Therefore, elucidating the relationship between its microstructure and optical properties is of significant importance for both mineralogy and materials science.

[a] Department of Applied Chemistry, Faculty of Science and Technology, Keio University, 3-14-1 Hiyoshi, Kohoku-ku, Yokohama 223-8522, Japan.

†Electronic Supplementary Information (ESI) available: Photographs of brilliantly colored regions (blue, green, and red) in Ethiopian and Australian black opals with corresponding color coordinates plotted on the Commission Internationale de l'Edairage (CIE) chromaticity diagram (Fig. S1); Reflectance spectra from various opals (Fig. S2); Cross-sectional SEM images of Ethiopian opal after sequential etching treatments with hydrofluoric acid (HF) (Fig. S3); XRD patterns of Ethiopian opal, black opal, and a cristobalite reference (Fig. S4); A high-angle annular dark-field (HAADF) image with TEM-EDS elemental mapping images for an FIB-cut sample of Ethiopian opal (Fig. S5); Schematic illustrations of the experimental setup for reflectance spectra and a typical reflectance spectrum of the reference light irradiated on a white polytetrafluoroethylene (PTFE) plate (Fig. S6); Photographs showing the positions for transmission spectra measurements of Ethiopian and black opals (Fig. S7). See DOI: 10.1039/x0xx00000x

View Article Online
DOI: 10.1039/D5TC01380A





Artificial photonic crystals that enable precise light control are vital for diverse optical applications. The coexistence of transparency and vivid color in Ethiopian opal suggests a novel optical architecture for advanced light manipulation. Consequently, this research aims to characterize the microstructure of Ethiopian opal and elucidate the mechanism that harmonizes its high transparency with its vivid structural color. Finally, this study demonstrates that a type of opal formed through geological processes offers significant insights for materials chemistry.

## Results and Discussion

As shown in Fig. 1a, b, Ethiopian opal uniquely combines vivid structural coloration with high transparency. We confirmed that the reflection spectra corresponding to the vivid colors are characterized by an extremely narrow full-width at half-maximum (FWHM) as compared to other opal colors (Fig. 1c and Figs. S1 and S2 in the Supporting Information (SI)). Their superior transparency is evident from their transmission spectra when compared with those of Australian black opal (Fig. 1d). The peak observed around 490 nm in the transmission spectrum likely originates from light reflection at the back of the sample (Fig. 1c, d).

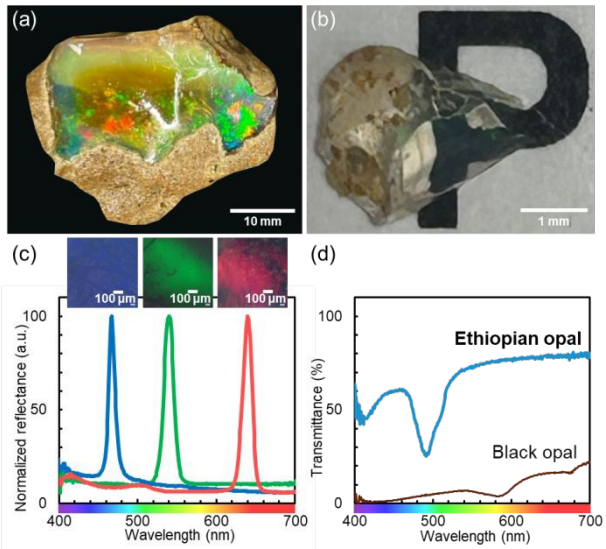


Fig. 1 (a, b) Photographs and (c) the normalized reflectance spectra with photos of blue, green, and red parts of Ethiopian opal. (d) The transmittance spectra of a blue part of Ethiopian opal and a white part of black opal dried in a vacuum for 336 h.

Figure 2 shows the microstructure of observed electron microscopies of Ethiopian opal. In the original cross section observed by scanning electron microscopy (SEM), the distinct colloidal particle arrangement typical of conventional opal was not observed (Fig. 2a). Due to the small density differences within the periodic structure of Ethiopian opal, it has not previously been possible to obtain clear information from SEM images. Therefore, in this study, the details were characterized by combining the elucidation of the overall periodic structure consisting of colloidal particles through transmission electron microscopy (TEM) with the observation of constituent nanoparticles through SEM. The TEM images of thin sections prepared by focused ion-beam (FIB) cutting indicate similar periodic arrangements of colloidal particles (Fig. 2d–f). The periodicity of several hundred nanometers correlates with the observed structural color. Notably, the lattice contrast remains subtle due to the presence of a cement material filling the interstitial spaces. More intriguingly, the electron density of the particle regions is lower than that of the surrounding cement regions—a structural configuration diametrically opposed to that of typical opal. The presence of the colloidal particles was also confirmed by SEM observation on a fracture surface exposed after etching treatment with hydrofluoric acid (Fig. 2b). Although the periodic array was disordered, spheres as the colloidal particles with a diameter of several hundred nanometers were revealed through the partial dissolution of their interior. The dissolution of the cores suggests that the density of interior of the spheres is lower than that of the interstitial region. These observations suggest that Ethiopian opal possesses a structure with an extremely small refractive index difference between the colloidal particles and the cementitious matrix.

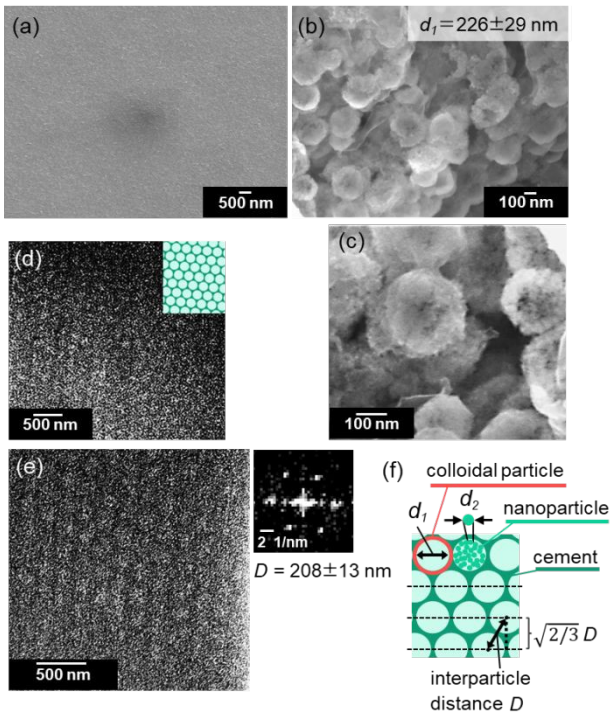


Fig. 2 SEM images (a) before and (b, c) after the etching treatment, (d, e) TEM images with a schematic illustration and the fast Fourier transform (FFT) pattern of an FIB-cut thin plate (thickness: 260 nm), and (f) a schematic illustration of a green part of Ethiopian opal. *D* represents the center-to-center distance, while $d_1$ and $d_2$ represent the diameters of the colloidal particles and nanoparticles, respectively. Brighter areas of the particle regions in TEM images mean lower electron density than that of the surrounding cement regions.

View Article Online
DOI: 10.1039/D5TC01280A





In the transmission spectrum of a sample 1 mm thick (Fig. 1d), the average transmittance was approximately 65%. Assuming that $D$ = 230 nm, a single period (layer spacing) corresponds to $\sqrt{(2/3)}D$ (Fig. 2f). Consequently, the number of periods, $N$, in the 1 mm sample is calculated to be ~5300. By neglecting light absorption and multiple reflections, the reflectance per period is estimated from the transmittance to be $8.1 \times 10^{-5}$, indicating an exceptionally low value. Based on the principle of the Fresnel reflection, this extremely low reflectance implies that Ethiopian opal features a structure with a significantly smaller refractive index difference as compared to other typical opals, highlighting its unique structural characteristic.

As shown in Fig. 2c, the presence of nanoparticles in the colloidal particles was revealed after the etching treatment with hydrofluoric acid. Figure 3 also shows that the colloidal particles are composed of primary nanoparticles approximately 20 nm in diameter, with distinct voids observed among them. The difference between the interior and the interstitial region was not observed before the etching treatment. The partial dissolution suggests that the density of nanoparticle aggregation in the interior of the colloidal particles is lower than that of the interstitial region (Fig. 2f). Nitrogen adsorption-desorption isotherms confirmed that these mesopores are approximately 6 nm in size (Fig. 3b). The space among the nanoparticles in the colloidal particles corresponds to the mesopore. The high porosity of these colloidal particles (Fig. 3c) results in an effective refractive index lower than that of the cement region. Furthermore, the inside regions of the colloidal spheres were found to be easily dissolved by the etching treatment due to the lower density (Fig. 2c and Fig. S3 in the SI).

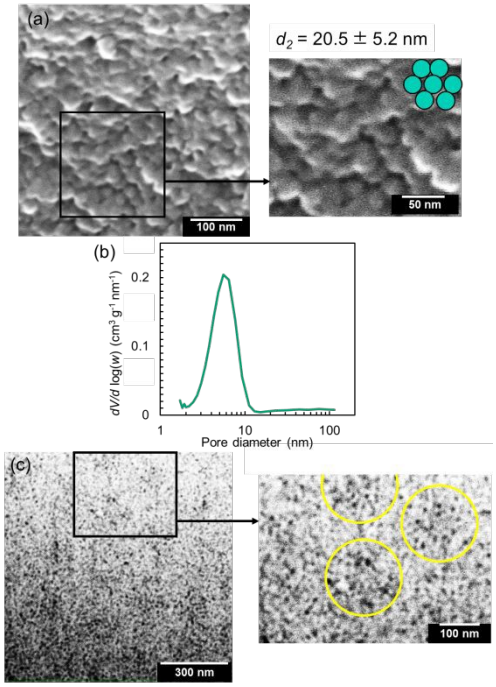


Fig. 3 (a) Enlarged SEM and (c) TEM images of a green part of Ethiopian opal with (b) a pore-size distribution evaluated by the nitrogen adsorption-desorption technique. Yellow circles indicate an area with a high concentration of voids.

The X-ray diffraction (XRD) pattern exhibits weak peaks not typically observed in purely amorphous silica, suggesting a degree of short-range ordering or incipient crystallization (Fig. S4 in the SI), which is consistent with previous reports.[14,16,18,23] The elemental analysis suggested a larger concentration of fluorine in the cement region than in the colloidal particles (Fig. S5 in the SI). On the other hand, no transition metals involved in coloration were detected.

The formation mechanism of these cemented opal structures is generally attributed to the following process: after the deposition of colloidal silica spheres, the interstitial voids are occupied by hydrated amorphous silica. This precursor then undergoes a prolonged and continuous impregnation with soluble silica, eventually leading to the solidification of the entire structure through a cementing process.[15] However, the structure observed in this study exhibited a higher density in the cement regions than in the colloidal particles. It is unlikely that such an inverse opal structure would form through this conventional mechanism, given that both the particles and the cement consist of nearly identical silica compositions. Therefore, a novel process is required to explain the formation of Ethiopian opal. Based on the results in this work, we propose the following formation mechanism for this unique architecture, as shown in Fig. 4. Initially, a periodic array is formed through the sedimentation of colloidal particles like a normal opal. According to the elemental mapping, their surfaces are inferred to be enriched with fluorine as an impurity. The fact of the partial crystallization suggests that the opal structure was subjected to geological compression and thermal fusion. The presence of fluorine likely lowers the softening temperature of the shell layer of particles,[24] causing the formation of a continuous cementitious matrix with a higher density through geological metamorphism. Finally, an "ill-defined" inverse opal structure is developed with the remaining porous regions in the core of the colloidal particles.

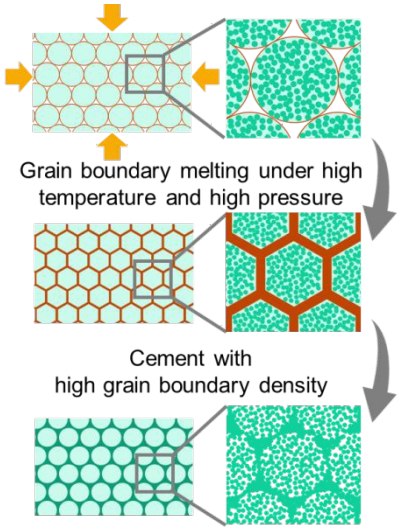


Fig. 4. Schematic illustration of the proposed formation mechanism of Ethiopian opal.

View Article Online
DOI: 10.1039/D5TC01280A

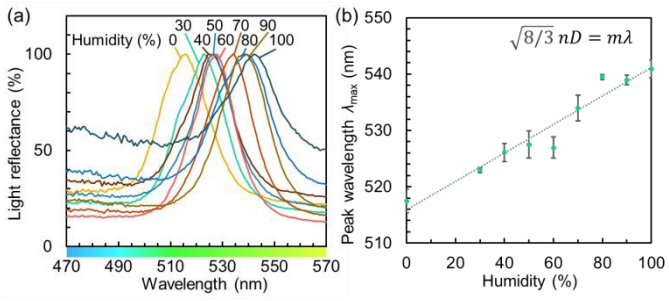


Fig. 5. (a) Changes in reflection spectra under different humidity levels and (b) relationship between humidity and reflection peak wavelength.

The presence of nano-sized pores triggers capillary water condensation even under low-humidity conditions. This condensation increases the effective refractive index of the colloidal particles, thereby shifting the reflected wavelength and altering the hue of the structural colors. As illustrated in Fig. 5, we confirmed a distinct spectral shift in a green specimen of Ethiopian opal in response to humidity variations. Our results demonstrate this shift, as compared to existing humidity-sensing materials utilizing similar capillary condensation,[25,26] Ethiopian opal functions a broader response range and a narrower half-width in static environments. Specifically, the hierarchical architecture—incorporating pores approximately 6 nm in diameter—enables high sensitivity to humidity. The relationship between humidity and reflection peak wavelength remained unchanged even after the humidity had fluctuated at least five times. Moreover, the specific optical property was not degraded by heating at ~100 ˚˚˚ C. Thus, Ethiopian opal exhibits function as a naturally occurring, colorimetric humidity sensor, where its nanostructured porosity dictates its responsive optical properties. However, based on the variation in wavelength at a constant humidity level, it is considered difficult to detect humidity changes of less than 5%.

To theoretically investigate this phenomenon, we model the refractive index of Ethiopian opal. The reflection wavelength ($\lambda$) for a colloidal photonic crystal is described by the Bragg-Snell law:

$$\sqrt{8/3\,(n^2 - \sin^2\theta)}D = m\lambda\,,$$

where $\vartheta$ is the angle of view, and $m$ is the order of the Bragg–Snell reflection. The reflection wavelength shifted from 517 to 541 nm as the condition changed from a dry state to 100% humidity. Assuming an interparticle distance of $D$ = 230 nm, this shift indicates that the effective refractive index of the entire system, $n_{eff}$, changed from 1.38 to 1.44 based on the Bragg-Snell law. Next, the effective refractive index $n_{eff}$ in the dry state can be expressed by the following equation,

$$n_{eff} = \sqrt{(n_p^2\varphi_p + n_c^2(1-\varphi_p))},$$

where $\varphi_p$ is the volume fraction of the colloidal particles and $n_p$ and $n_c$ are the refractive indices of the colloidal particles and the cementitious material, respectively. Point counting of the periodically structured region in Fig. 2c revealed that the cross-sectional area fraction of the colloidal particles was 0.54. Approximating the volume fraction to $\varphi_p \fallingdotseq 0.5$ for simplicity and applying the dry-state $n_{eff}$ = 1.38, we obtain the following relationship,

$$1.38 = \sqrt{(0.5n_p^2 + 0.5n_c^2)}.$$

Furthermore, according to the principle of the Fresnel reflection, the relationship between reflectance ($R$) and the refractive indices is given by,

$$R = \left(\frac{n_c - n_p}{n_c + n_p}\right)^2.$$

From our earlier estimation based on the transmission spectra, the reflectance is known to be $R$ = 8.1×10$^{-5}$. By solving these two equations simultaneously, we calculated that $n_p$and $n_c$ are 1.37 and 1.39, respectively. The refractive index difference between the two is $\Delta n$ = 0.02, which is significantly smaller than that of other opals. This result successfully provides a theoretical basis for the exceptionally high transparency of Ethiopian opals.

We further estimated the volume fraction of the total silica, $\varphi_s$, in Ethiopian opal. Using a refractive index of 1.46 for silica and 1.00 for air and applying the dry-state effective refractive index of 1.38, we calculated $\varphi_s$= 0.81. Assuming that the air in the voids is entirely replaced by water (refractive index: 1.33), the effective refractive index increases to 1.44. This value perfectly matches the wet-state effective refractive index derived earlier from the Bragg–Snell equation, demonstrating the consistency of our model. Finally, assuming the specific gravity of amorphous silica to be 2.2 g/cm³ and that of water to be 1.0 g/cm³, the estimated mass ratio is silica : water ≈ 9 : 1. This is in excellent agreement with the approximately 10 wt% mass increase observed when Ethiopian opals are immersed in water,[14] further confirming the validity of the parameters obtained in this study.

## Conclusions

This study has elucidated the unique optical mechanism and formation process of Ethiopian opal, characterized by its high transparency and vivid structural coloration. Our microstructural analysis revealed that these properties originate from a subtly defined inverse opal architecture, where colloidal particles are embedded within a higher-density cementitious matrix. This structural configuration creates an extremely low refractive index contrast at each interface, allowing for high optical transmittance while simultaneously producing a sharp reflection spectrum through the interference of thousands of layers. Furthermore, we found that the





 

View Article Online
DOI: 10.1039/D5TC01389A

hierarchical porosity within these particles, featuring mesopores of approximately 6 nm, facilitates capillary water condensation even at low humidity levels. This property allows the material to function as a sensitive, naturally occurring colorimetric humidity sensor. These findings not only resolve a long-standing mystery regarding the optical properties of Ethiopian opal but also provide a novel design principle for developing highly transparent, responsive photonic materials based on low-contrast, multilayer interference.

## Experimental

### Materials

Samples of Ethiopian opals from Ethiopia, black opals and picture opals from Australia were used. Ethiopian opal in matrix was purchased from Tenkawa crystal. Black opals and picture opals in matrix were purchased from Yotosha.

### Analytical methods

The colors were evaluated by the CIE chromaticity diagram using image analysis software (ImageJ Fiji). The reflectance and transmittance spectra were obtained by a combination of a digital microscope (VHX-970 F, Keyence) and a microchannel spectrometer (Photonic multi-channel analyzer PMA-12, Hamamatsu Photonics). White light from a light-emitting diode (LED Luminar Ace LA-HDF158A, Hayashi) projected on a white plate (polytetrafluoroethylene, PTFE) was used as the reference for reflectance measurements (Fig. S6 in the SI). For transmittance measurements, the probe area was restricted by a 2 mm diameter pinhole. The reference signal was first collected through the open pinhole, after which the sample was mounted to cover the aperture entirely (Fig. S7 in the SI). The reference light and the transmitted light from the samples were measured under the same magnification.

Samples were fractured or buried in epoxy resin (C&A) and polished to expose a cross section. For the samples embedded in resin, the surfaces were first etched in a 1.0 vol% aqueous hydrofluoric acid (FUJIFILM Wako Pure Chemical) solution for 30 s, followed by a second etching step in a 0.1 vol% solution for 5 min to reveal the internal colloidal structures and then coated with osmium for detailed observation using a scanning electron microscope (SEM, JEOL JSM-7100F) operated at 15.0 kV. $d_1$ and $d_2$ were randomly measured ($n$ = 50) with SEM images using the image analysis software. Detailed internal observation and elemental mappings were performed by transmission electron microscopy-energy dispersive X-ray spectroscopy (TEM-EDS, FEI Tecnai Osiris) operated at 200 kV after being processed by focused ion beam (FIB, FEI Quanta 3D FEG). $D$ was measured by the fast Fourier transform (FFT) pattern obtained from the squared region of the TEM image. Powder X-ray diffraction (XRD) measurements were conducted using a diffractometer (Bruker, D8 ADVANCE Eco) with Cu-Kα radiation in a continuous scan mode. Data were collected over a $2\vartheta$ range of 10°–65° with a step size of 0.0195°. The pore-size distribution of the ground samples was determined by nitrogen adsorption using a surface area and porosimetry analyzer (3Flex, Micromeritics). To evaluate humidity dependence, the samples were placed in a small environmental chamber (SH-242, ESPEC) at 25°C with the relative humidity (RH) varied from 30% to 100%. Since the peak shift saturated within one hour, reflectance spectra were recorded immediately after the samples had been equilibrated for at least 1 h at each humidity level.

## Author contributions

HI supervised the project. NH, YO, and HI designed the experimental procedures of microstructure analysis. NH and HI observed the structure of Ethiopian opals and analyzed the results. All authors reviewed the results and approved the final version of the manuscript.

## Conflicts of interest

There are no conflicts to declare.

## Acknowledgements

This work was supported by JSPS KAKENHI grant number JP21H01627.

## Data availability

The authors declare that the data supporting the findings of this study are available within the paper and its Supplementary Information file. Raw data files are available from the corresponding author upon reasonable request.

## Declaration of Generative AI and AI-assisted technologies in the writing process

During the preparation of this work, the authors used Gemini (Google) in order to improve language and readability. After using this service, the authors reviewed and edited the content as needed and take full responsibility for the content of the publication.

## Notes and references

1 S. Kinoshita and S. Yoshioka, *ChemPhysChem*, 2005, **6**, 1442–1459.
2 S. Kinoshita, S. Yoshioka and J. Miyazaki, *Rep. Prog. Phys.*, 2008, **71**, 076401.
3 A. G. Dumanli and T. Savin, *Chem. Soc. Rev.*, 2016, **45**, 6698–6724.
4 J. V. Sanders, *Nature*, 1964, **204**, 1151–1153.
5 J. Sanders and J. V. Sanders, *J. Phys. Colloq.*, 1985, **46**, C3-1-C3-8.
6 F. Marlow, Muldarisnur, P. Sharifi, R. Brinkmann and C. Mendive, *Angew. Chem., Int. Ed.*, 2009, **48**, 6212–6233.
7 J. B. Jones and E. R. Segnit, *J. Geol. Soc. Aust.*, 1971, **18**, 57–67.
8 E. Gaillou, G. Fritsch, B. Aguilar-Reyes, B. Rondeau, J. Post, A. Barreau and M. Ostroumov, *Am. Mineral.*, 2008, **93**, 1865–1873.
9 Z. Cai, Z. Li, S. Ravaine, M. He, Y. Song, Y. Yin, H. Zheng, J. Teng and A. Zhang, *Chem. Soc. Rev.*, 2021, **50**, 5898–5951.
10 Y. Chen, X. Ye, Z. Zheng, L. Wang and S. Cao, *Solar RRL*, 2021, **5**, 2000541.
11 N. Vogel, M. Retsch, C. A. Fustin, A. Del Campo and U. Jonas, *Chem. Rev.*, 2015, **115**, 6265–6311.

View Article Online
DOI: 10.1039/D6TC01280A

12. I. B. Burgess, M. Loncar, J. Aizenberg, *J. Mater. Chem. C*, 2013, **1**, 6075.
13 M. Liesegang and R. Milke, *Am. Mineral.*, 2014, **99**, 1488–1499.
14 B. Rondeau, E. Fritsch, F. Mazzero, J.-P. Gauthier, B. Cenki-Tok, E. Bekele and E. Gaillou, *Gems Gemol.*, 2010, **46**, 90–105.
15 R. K. Iler, *Nature*, 1965, **207**, 472–473.
16 E. Martin and E. Gaillou, *Am. Mineral.*, 2018, **103**, 803–811.
17 I. Maurin, E. Moufarej, A. Laliotis and D. Bloch, *J. Opt. Soc. Am. B*, 2015, **32**, 1761–1772.
18 K. Zhao and F. Bai, *Minerals*, 2020, **10**, 625.
19 U. G. K. Wegst, H. Bai, E. Saiz, A. P. Tomsia and R. O. Ritchie, *Nat. Mater.*, 2015, **14**, 23–36.
20 H.-B. Yao, J. Ge, L.-B. Mao, Y.-X. Yan and S.-H. Yu, *Adv. Mater.*, 2014, **26**, 163–188.
21 M. A. Meyers, P.-Y. Chen, A. Y. M. Lin and Y. Seki, *Prog. Mater. Sci.*, 2008, **53**, 1–206.
22 N. Hizukuri, Y. Oshima, Y. Yagi, H. Sasazawa, Y. Oaki, H. Tsuda and H. Imai, *Sci. Rep.*, 2025, **15**, 12345.
23 A. A. Ejigu, D. G. Ketemu, S. A. Endalew and W. Y. Assen, *J. Spectrosc.*, 2022, **2022**, 3194151.
24 K. Schuster, S. Grimm, A. Kalide, J. Dellith, M. Leich, A. Schwuchow, A. Langner, G. Schötz and H. Bartelt, *Opt. Mater. Express*, 2015, **5**, 887–897.
25 Y. Hao, Y. Han, H. Luo and X. Huang, *Opt. Mater.*, 2026, **169**, 117599.
26 Y. Chen, Z. H. Zuo, Z. Q. Liu and Y. Yin, *Small*, 2022, **18**, 2204484.



View Article Online
DOI: 10.1039/D6TC01280A

The authors declare that the data supporting the findings of this study are available within the paper and its Supplementary Information file. Raw data files are available from the corresponding author upon reasonable request.